

## Supplementary Information

### Enhancing energy storage performances in $\text{Bi}_{0.5}\text{Na}_{0.5}\text{TiO}_3$ -based dielectric ceramics via modulating polymorphic polar nanoregions

Xiaoyan Dong<sup>1</sup>, Xiaojun Wu<sup>1</sup>, Xiang Lv<sup>1\*</sup>, Jiagang Wu<sup>1\*</sup>

<sup>1</sup> College of Materials Science and Engineering, Sichuan University, Chengdu 610065, P. R. China

\*Corresponding authors.

E-mail: lvxiang@scu.edu.cn (X. Lv), msewujg@scu.edu.cn (J. Wu)

## 1. Experimental procedure

Relaxor ferroelectrics of  $(1-x)\text{Bi}_{0.94}\text{Na}_{0.94}\text{Ba}_{0.06}\text{TiO}_3-x\text{Sr}(\text{Ni}_{1/3}\text{Nb}_{2/3})\text{O}_3$  (abbreviated as 100xSNN,  $x = 0.06, 0.09, 0.12,$  and  $0.15$ ) were fabricated via the conventional solid-state reaction. The high-purity powders of  $\text{Na}_2\text{CO}_3$  ( $\geq 99.8\%$ ),  $\text{SrCO}_3$  ( $\geq 99\%$ ),  $\text{BaCO}_3$  ( $\geq 99\%$ ),  $\text{NiO}$  ( $\geq 99\%$ ),  $\text{Bi}_2\text{O}_3$  ( $\geq 99\%$ ), and  $\text{Nb}_2\text{O}_5$  ( $\geq 99.95\%$ ) were adopted as the raw materials. Then these powders were accurately weighed and ball-milled for 12 h with  $\text{ZrO}_2$  balls and alcohol as medium. Subsequently, the mixtures were calcined at  $850\text{ }^\circ\text{C}$  for 4 h. A secondary ball-milling session for 12 h followed by the calcination. The resulting powders were combined with 8 wt% polyvinyl alcohol (PVA) and formed into pellets, 8 mm in diameter and 1 mm thick, using uniaxial pressing at 200 MPa. Finally, the above samples were naturally sintered at  $1100\text{-}1150\text{ }^\circ\text{C}$  for 2 h after the removal of PVA.

The crystal structures of the 100xSNN ceramics were analyzed by X-ray diffraction (XRD) (Bruker D8 Advance XRD, BrukerAXS Inc., Madison, WI,  $\text{CuK}_\alpha$ ). The selected area electron diffraction (SAED) was obtained by FEI Talos F200X. Due to the abnormal growth of grain size on the surface of ceramics after sintering, the sintered samples were polished and thermally etched at  $950\text{-}1100\text{ }^\circ\text{C}$  for 20 min depending on the composition. Then tested by scanning electron microscopy (FE-SEM, Model S4800, Hitachi, Japan) after platinum coating. The dielectric properties of the 100xSNN ceramics were measured using an LCR analyzer (HP, 4980, Agilent) after polished to a thickness of  $0.80 \pm 0.01$  mm and coated silver electrode with a diameter of approximately 7.8 mm. To characterize the energy storage performance, the sintered samples were polished to a thickness of  $0.070 \pm 0.01$  mm and coated with silver electrodes with a diameter of approximately 1.2 mm. Then, the silver electrode was formed by firing at  $600\text{ }^\circ\text{C}$  for 30 minutes for electrical measurements. The polarization electric field ( $P$ - $E$ ) loops were obtained by a ferroelectric tester (RT66, Radiant

Technologies, NM, USA). The domain structures were investigated using a piezoresponse force microscopy (PFM, MFP-3D, USA) equipped with Pt/Ir-coated conductive tips (Nanosensors, Neuchatel, Switzerland).

The breakdown behavior was simulated by a phase field breakdown model. Herein, a scalar field  $s(\mathbf{x}, t)$  is introduced to characterize the breakdown state of the BNBT and 12SNN ceramics [1]. The scalar field  $s(\mathbf{x}, t)$  is a function related to spatial position and time, with values ranging from 0 to 1. To characterize the conductive behavior of ceramics, the dielectric constant is utilized as the primary descriptor. The initial dielectric constant,  $\varepsilon_r(0)$ , is set as  $\varepsilon_r(0)/\delta$ , where  $\delta$  is designated as a sufficiently small value (**Table 1**). Therefore,  $\varepsilon_r$  is a continuous function of the field variable  $s$  and can be expressed as:

$$\varepsilon(s) = \frac{\varepsilon_{intact}}{f(s) + \delta}, \quad (1)$$

where  $f(s) = 4s^3 - 3s^4$ . To quantitatively describe the dielectric breakdown behavior, the  $\varepsilon_r(0)$  of grain boundaries is set to 10/1 of the grain size. In this research, the grains were considered to have significant ferroelectric properties. Correspondingly, the  $\varepsilon_r$  is related to the electric field and can be described by the Johnson approximation model [2]. For the grain boundary, the  $\varepsilon_r$  is independent of the electric field. Hence, the relationship between the  $\varepsilon_r$  of ceramic and the electric field can be expressed by the following formula:

$$\varepsilon(E) = \begin{cases} \varepsilon_g(0)/(1 + kE^2)^{2/3} & , \quad \text{grain} \\ \varepsilon_{gb}(E) & , \quad \text{grain boundary} \end{cases}, \quad (2)$$

where  $k$  denotes a material constant related to Johnson's parameter  $\beta$  by  $k = 3[\beta(\varepsilon_0\varepsilon_{g/gb}(0))^3]$ . The  $\varepsilon_g(0)$ , and  $\varepsilon_{gb}(0)$  are the  $\varepsilon_r$  of grain and grain boundary, respectively. The variation in the  $s(\mathbf{x}, t)$  can be evaluated by observing changes in the total potential energy of the system. The total potential energy of the system primarily comprises three components: electrostatic energy ( $W_{es}$ ), damage energy ( $W_d$ ), and phase boundary gradient energy ( $W_i$ ). The corresponding formula is as follows:

$$W(\mathbf{E}, s, \nabla s) = W_{es}(\mathbf{E}, s) + W_d(s) + W_i(\nabla s), \quad (3)$$

Where  $W_{es}(\mathbf{E}, s) = -\frac{\varepsilon}{2} \mathbf{E} \cdot \mathbf{E}$ ,  $W_d(s) = W_c[1 - f(s)]$  ( $W_c$  denotes the critical density of electrostatic

energy), and  $W_i(\nabla s) = \frac{\Gamma}{4} \nabla s \cdot \nabla s$  [The electric field vector  $\mathbf{E}$  is related to the field of electric potential

$\phi(\mathbf{x}, t)$  ( $\mathbf{E} = -\nabla\phi$ ), the material parameter  $\Gamma$  can be approximately regarded as the breakdown energy].

By further integrating the above equations over the entire solution domain, the following energy function can be derived:

$$\Pi[s, \phi] = \int_{\Omega} [W_{es}(\mathbf{E}, s) + W_d(s) + W_i(\nabla s)] dV, \quad (4)$$

where assuming a linear kinetics relationship between the propagation speed of the breakdown and

the energy variation concerning the  $s$  ( $\frac{\partial s}{\partial t} = -m \frac{\delta \Pi}{\delta s}$ ), based on the aforementioned equation, the evolution equation for variables can be derived as follows:

$$\frac{1}{m} \frac{\partial s}{\partial t} = \frac{3\varepsilon_0 \varepsilon'_g(s)}{4k} [(1 + kE^2)^{\frac{2}{3}} - 1] + \frac{\Gamma_g}{\alpha^2} f'(s) + \frac{\Gamma_g}{2} \nabla^2 s, \text{ the grain} \quad (5)$$

$$\frac{1}{m} \frac{\partial s}{\partial t} = \frac{\varepsilon_0 \varepsilon'_{gb}(s)}{2} E^2 + \frac{\Gamma_{gb}}{\alpha^2} f'(s) + \frac{\Gamma_{gb}}{2} \nabla^2 s, \text{ the grain boundary} \quad (6)$$

where the  $m$  is a parameter that characterizes the breakdown evolution rate. The  $\alpha$  is a length scale to regularize. For the convenience of analysis, further normalization is applied, yielding the dimensionless governing equation as follows:

$$\begin{cases} \bar{\nabla} [\varepsilon_g(s) (1 + k \bar{\nabla} \bar{\phi} \cdot \bar{\phi})^{\frac{1}{3}}] = 0 \\ \frac{\partial s}{\partial t} = -\frac{3\varepsilon'_g(s)}{4k} ((1 + k \bar{\nabla} \bar{\phi} \cdot \bar{\nabla} \bar{\phi})^{\frac{2}{3}} - 1) + f'(s) + \frac{1}{2} \bar{\nabla}^2 s \end{cases}, \text{ the grain} \quad (7)$$

$$\begin{cases} \bar{\nabla} \cdot [\varepsilon_{gb}(s) \bar{\nabla} \bar{\phi}] = 0 \\ \frac{\partial s}{\partial t} = -\frac{\varepsilon'_{gb}(s)}{2} \bar{\nabla} \bar{\phi} \cdot \bar{\nabla} \bar{\phi} + f'(s) + \frac{1}{2} \bar{\nabla}^2 s \end{cases}, \text{ the grain boundary} \quad (8)$$

Under the correct boundary and initial conditions, Eqs. (7) and (8) can be applied to the solution of

dimensionless unknown fields  $\phi(\mathbf{x}, t)$  and  $s(\mathbf{x}, t)$ . Corresponding parameters used in the simulations are summarized in **Table 1**.

**Table 1** The parameters used in the phase-field simulations for breakdown behavior.

Parameters	Value	Definition
$\beta$	$1 \times 10^{10} \text{ Vm}^5\text{C}^{-3}$	LGD parameter
$\alpha$	20 nm	Length scale to regularize
$\Gamma_g$	$3.52 \times 10^{-8} \text{ J m}^{-1}$	Constant coefficient related to the breakdown energy of the grains
$\Gamma_{gb}$	$3.52 \times 10^{-9} \text{ J m}^{-1}$	Constant coefficient related to the grain boundaries
$\Gamma_{gb}$	$1.41 \times 10^{-8} \text{ J m}^{-1}$	Grain boundaries
$\varepsilon_g(0)$	2140	The $\varepsilon_r$ of the grains (BNBT)
$\varepsilon_{gb}(0)$	214	The $\varepsilon_r$ of the grain boundaries (BNBT)
$\varepsilon_g(0)$	1760	The $\varepsilon_r$ of the grains (12SNN)
$\varepsilon_{gb}(0)$	176	The $\varepsilon_r$ of the grain boundaries
$\varepsilon_0$	$8.854 \times 10^{-12} \text{ CV}^{-1}\text{m}^{-1}$	Permittivity of space
$\delta$	$10^{-4}$	A small positive constant meant to numerical stability
$m$	$5 \times 10^{-7} \text{ m}^2\text{s}^{-1}\text{N}^{-1}$	Mobility parameter related to speed of the breakdown propagation

## 2. Results and discussion

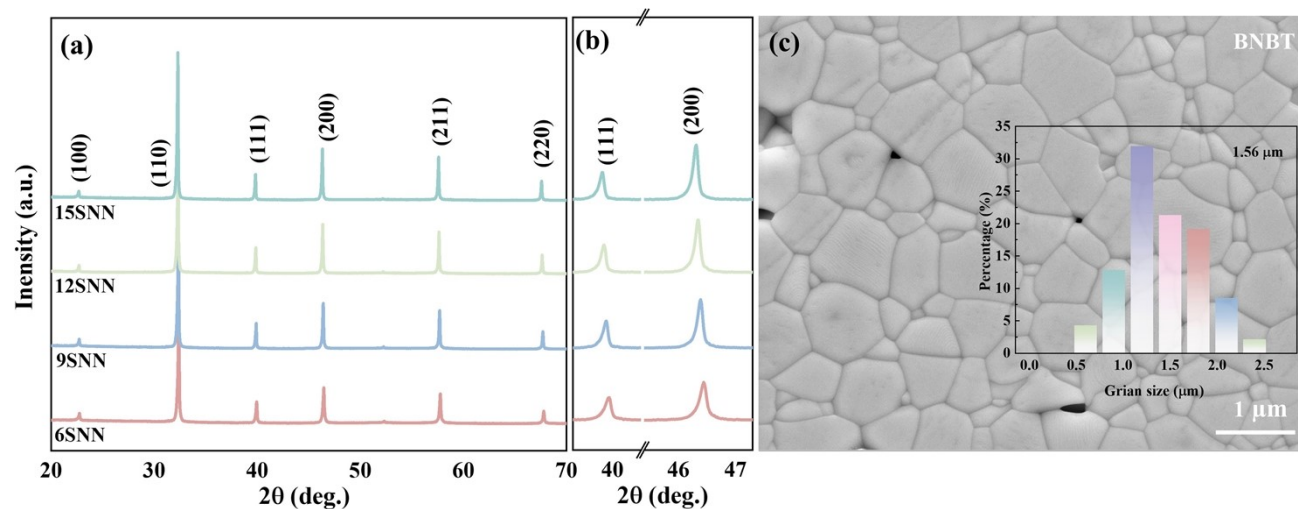


**Fig. S1** (a) Room temperature XRD patterns of 100xSNN ceramics; (b) enlarged XRD patterns with  $2\theta = 39.3\text{-}40.5^\circ$  and  $45.4\text{-}47.3^\circ$ ; (c) SEM image of BNBT ceramic (Inset gives the grain size distribution).

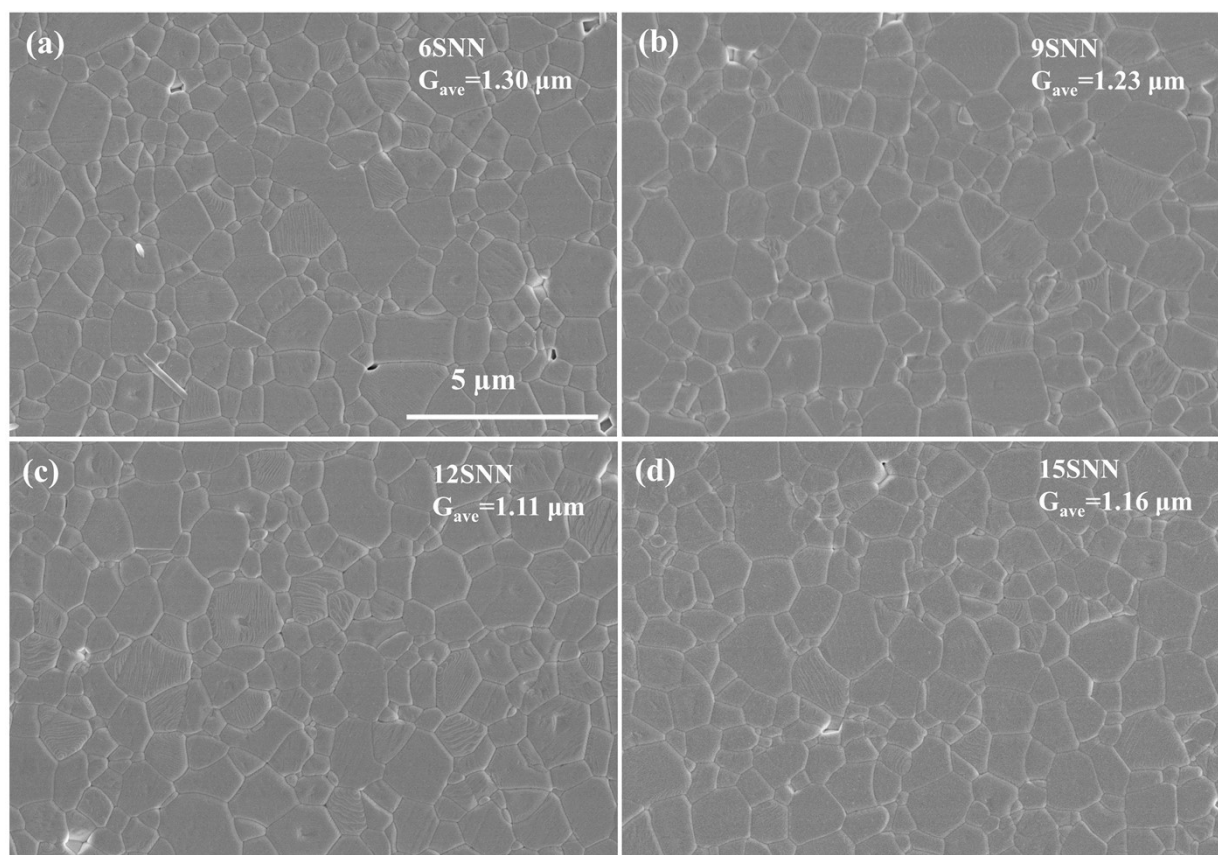


**Fig. S2** (a)-(c) FE-SEM images of 100xSNN ceramics. All images in have the same scale bar.

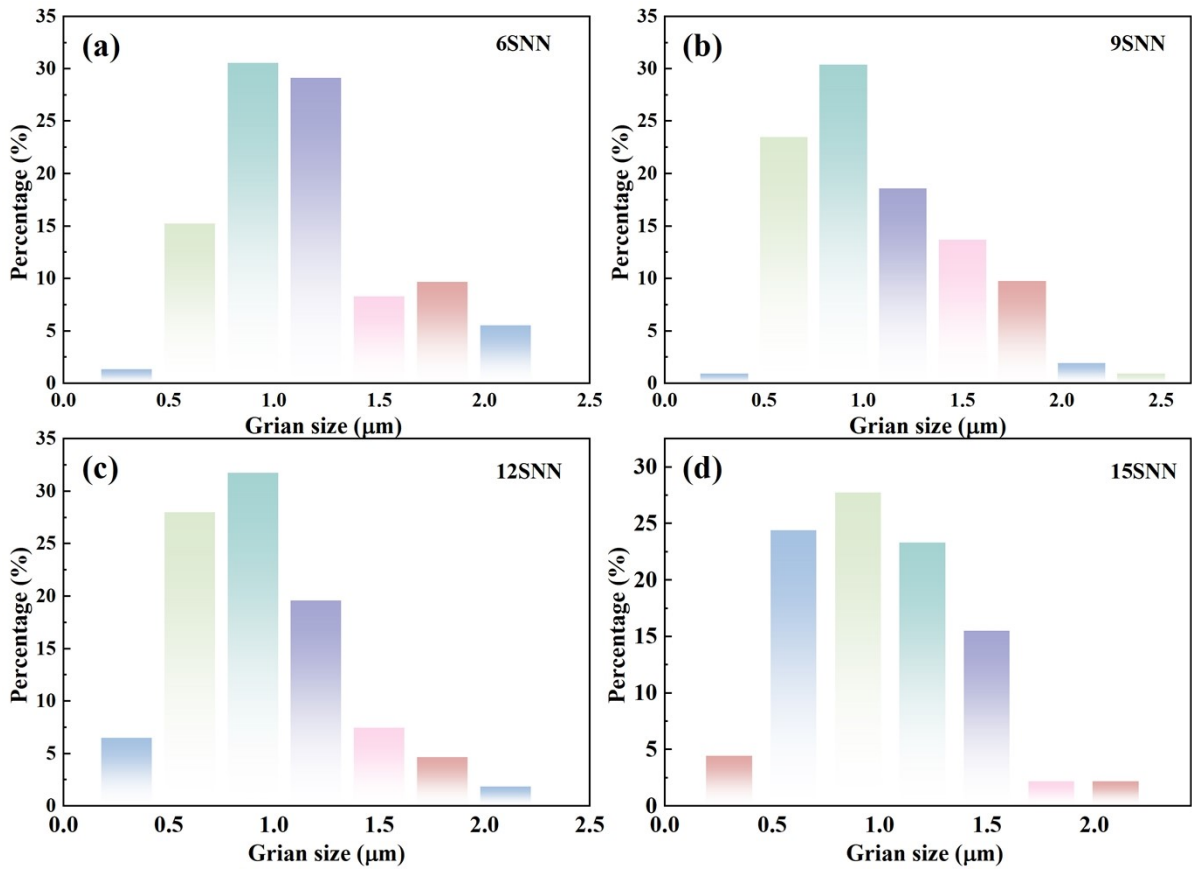


**Fig. S3** (a-d) The statistical histogram of grain size distribution of 100xSNN ceramics.

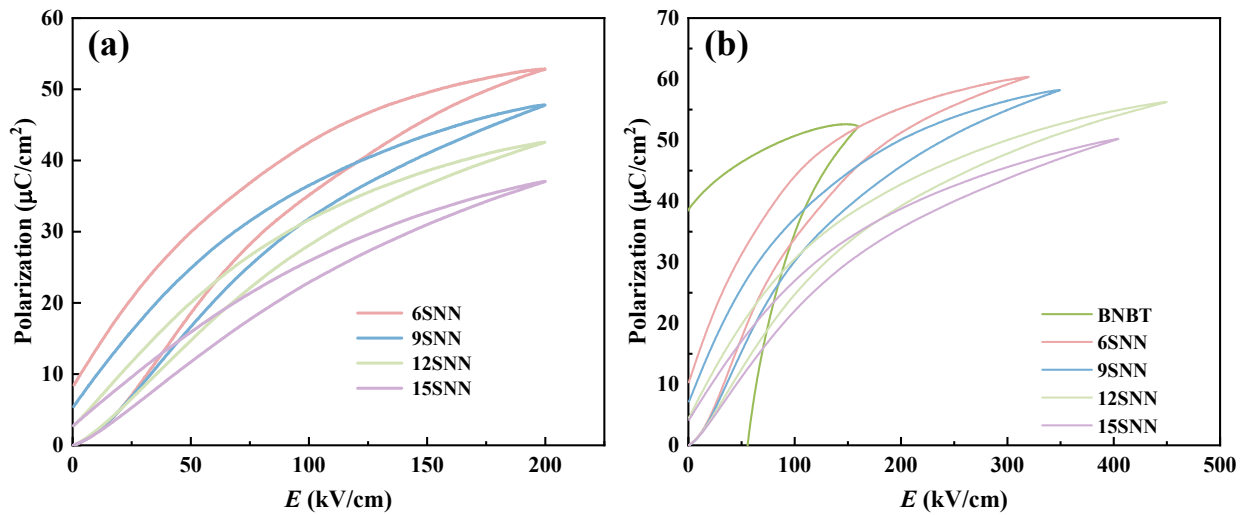


**Fig. S4** (a) Unipolar  $P-E$  loops of 100xSNN ceramics at 200 kV/cm; (b) unipolar  $P-E$  loops for BNBT and 100xSNN ceramics under their maximum electric fields.

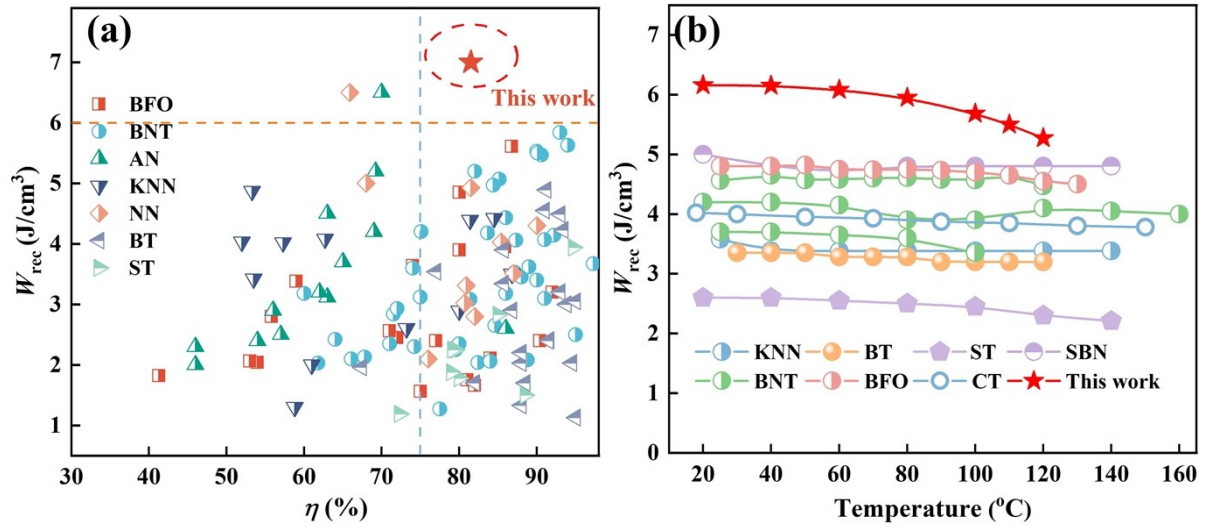


**Fig. S5** (a) Comparison of energy storage properties and (b) temperature stability of  $W_{\text{rec}}$  between 12SNN and some other lead-free systems (Abbreviated: KNN,  $\text{K}_{0.5}\text{Na}_{0.5}\text{NbO}_3$ ; BT,  $\text{BaTiO}_3$ ; ST,  $\text{SrTiO}_3$ ; SBN,  $\text{Sr}_{0.53}\text{Ba}_{0.47}\text{Nb}_2\text{O}_5$ ; BNT,  $\text{Bi}_{0.5}\text{Na}_{0.5}\text{TiO}_3$ ; BFO,  $\text{BiFeO}_3$ ; CT,  $\text{CaTiO}_3$ ).

## Reference

- [1] M. Khondabi, H. Ahmadvand, M. Javanbakht, *Adv. Theor. Simul.*, 2022, 6, 2200314-2200323.  
 [2] K. M. Johnson, *J. Appl. Phys.*, 1962, 33, 2826-2831.